[Frontiers in Bioscience 8, s982-991, September 1, 2003]

NUMERICAL FRAMEWORK MODELS OF SINGLE PROTON CONDUCTION THROUGH GRAMICIDIN

Mark F. Schumaker

Department of Mathematics and Center for Integrated Biotechnology, Washington State University, Pullman WA 99164-3113

TABLE OF CONTENTS

1. ABSTRACT

A framework model of single-proton conduction through gramicidin was previously designed to incorporate potentials of mean force and diffusion coefficients computed by the molecular dynamics simulations of Pomès and Roux (1). The resulting diffusion model was solved analytically using the lumped state approximation (LSA), allowing a detailed comparison to be made with conductance data from gramicidin A and two Trp→ Phe analogs (2). The comparison included a sensitivity analysis which required over 1 million current evaluations. A numerical method for constructing framework models is now introduced which involves finding the steady states of random walks using a trapezoid rule closely related to the rule for numerical integration. The method is described and then applied directly to the LSA. Convergence of the results to the analytical solution is seen as the number of random walk sites increase. The numerical method is then used to construct a more elaborate framework model which avoids the LSA. This is also in very good agreement with the analytical solution under the experimental conditions, confirming the accuracy of the LSA. The numerical method remains fast enough to allow an extensive comparison with conductance data.

2. INTRODUCTION

Molecular dynamics (MD) simulations give the most detailed theoretical representation of ion permeation, but there is a very large gap between times scales that can be simulated directly and those required to evaluate currents and perform detailed comparisons with conductance data. One way to overcome this gap in time scales is to project the results of the MD to diffusion models that can be used to rapidly calculate conductances. These *framework models* are designed to incorporate potentials of mean force and diffusion coefficients calculated by MD simulations. Detailed comparisons of the models with experimental conductances represent a very severe test of the precision of the energies computed in the simulations, providing corrective feedback for their design. At the same time, the simulations are already accurate enough to suggest hypotheses regarding the conduction mechanisms of ion channels.

The gramicidin monomer is a peptide with 15 alternating L and D amino acids. The structure of the conducting N-terminal to N-terminal dimer has been determined by NMR spectroscopy (3-4). The dimer forms a conducting channel in which the two monomers are identical β helices. The pore is about 25 Å long and 4 Å in diameter. The relative simplicity of this structure makes it a convenient testbed for developing models of proton permeation and a point of reference for the discussion of other, biologically important, proton channels (5). Pomès and Roux (1) performed MD simulations of gramicidin using the CHARMM force field. The simulated structure included the channel, 10 pore waters, and a cap of water molecules around each channel entrance. To investigate the mechanism of proton conduction, two sets of simulations were performed. One set included an excess proton in the pore while the other set included only the pore waters.

The potential of mean force for an excess proton in the pore is shown in Figure 1A. It was calculated as a function of the reaction coordinate μ^H, which is the axial component of the summed pore water dipole moment. This reaction coordinate has the advantage that it can be calculated unambiguously, even though the excess proton in the pore is not uniquely identified. At the same time, its values are proportional to a spatial coordinate: $\mu = -\mu_A{}^H$ corresponds to a proton at the channel entrance on side I (on the left) and $\mu^H = \mu_A{}^H$ corresponds to a proton at the channel entrance on side II (on the right). The proton PMF is a shallow potential well. There is a very high associated diffusion coefficient (6).

Potentials of mean force were also calculated for the pore waters without an excess charge (1). They are shown as the dots (PM6 waters) and the dashes (TIP3P waters) in Figure 1B. These simulations investigated the dynamics of water reorientation between conformations in which the water dipole moments are aligned towards one entrance or the other. They were also parameterized by the axial component of the summed pore water dipole moment, now denoted μ^d. Reorientation between these two configurations is thought to be mediated by a defect in the

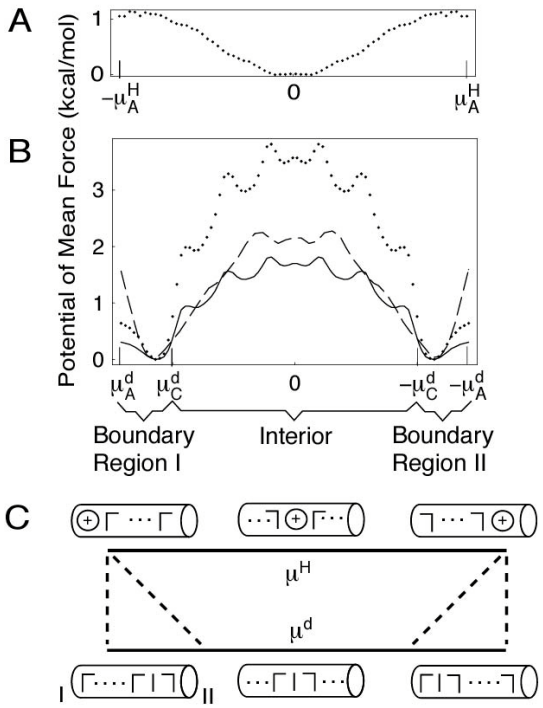

Figure 1. Molecular dynamics simulations of single proton conduction (4). (A) Proton potential of mean force (PMF). (B) Defect PMF. Dots give the potential calculated using PM6 waters and the dashed curves gives the potential calculated using TIP3P waters. The solid curve is the PM6 potential scaled to allow a fit to conductance data (10). Notice that the abscissa increases to the left. Boundary regions are the intervals $\mu_C^d < |\mu| < \mu_A^d$. (C) Simplified configuration space of the permeation mechanism suggested by the simulations. Cartoons illustrate the state of the channel near the ends and at the middle of each segment. The sketches of the water reorientation defects below the bottom segment are consistent with the suggestion of Pomès (6). Numerals on either end of the lower left cartoon indicate entrances on side I and II of the channel. Both μ^H and μ^d increase as the state diagram is traversed clockwise. Two pairs of dashed lines delimit families of transitions from the endpoints of the proton (or top) segment to the boundary regions on the defect (or bottom) segment.

water chain, about which the axial component of the water dipole moment turns. The lowest energy conformations, in the boundary regions, correspond to water columns that are nearly aligned, with defects only close to the channel entrances.

The MD with and without an excess proton in the pore suggests a mechanism of proton permeation through gramicidin, sketched in Figure 1C. Consider an excess proton which enters the channel through the entrance on side I. The center of excess charge may diffuse through the pore and leave the channel through the entrance on side II. The proton (or top) segment parameterizes this process. While in the channel, neighboring waters are aligned by the excess charge, although the strength of the correlation declines for waters well separated from the center of charge (7). When the proton leaves the channel, the remaining waters will remain partially aligned. The water column can be left in a range of states; the possible transitions are delimited by the dashed lines from the proton to the defect (or bottom) segment. The interval of states on the defect segment encompassed by these lines is boundary region II. It is delimited by its endpoints, $-\mu_C^d$ and $-\mu_A^d$.

The defect segment parameterizes water reorientation. The waters must now turn before their dipole moments will have a favorable energy of interaction with a new excess proton entering the pore through the entrance on side I. Consistent with the MD simulations (1), water reorientation in the model is mediated by a defect which diffuses over the potential barrier in Figure 1B. The alignment of waters shown in the cartoons below the defect segment in Figure 1C depicts a defect with a partial positive charge (8), although defects with a partial negative charge have also been suggested (9). When the channel is in boundary region I, the range of states delimited by dashed lines on the left, it is receptive to another proton entering the pore on side I.

The proton permeation mechanism suggested by Figure 1C is the basis of a framework model (2,6,10) which describes proton permeation through gramicidin A and analogs in which either one pair of tryptophans was replaced by phenylalanine (gramicidin B) or all four pairs of tryptophans were replaced by phenylalanine (gramicidin M). By describing proton entrance and exit only from the endpoints of the top segment, the model implicitly assumes that waters in the occupied pore are fully aligned by the excess charge. Despite the cartoons drawn below the bottom segment of Figure 1C, the mathematical model makes no assumption regarding the structure of the defect.

A detailed comparison was made between experimental and model proton conductances (2). Very good agreement was obtained with previous calculations of the electrostatic interaction between the tryptophan indoles and cations in the pore (11). The permeation mechanism suggested by Figure 1C describes at most only a single excess proton in the pore. A shoulder in the experimental data for gramicidin A and B separating regimes of conductance at high and low pH was interpreted as a transition to a conduction mechanism in which states with two or more protons in the pore are significant.

A fundamental assumption made by this framework model is that the dynamics of proton permeation and water reorientation can be adequately described by processes parameterized by single reaction coordinates. This is not the same as assuming that the dynamics are geometrically one dimensional. For example, the permeation pathway of a cation through gramicidin is thought to have a helical character because of the coordination of the cation with the helical peptide backbone. This helical character is simulated by the molecular dynamics. The full geometry of the simulation enters into the calculations of the potential of mean force and diffusion coefficients which are used by the framework model. The three dimensional geometry is therefore implicitly taken into account.

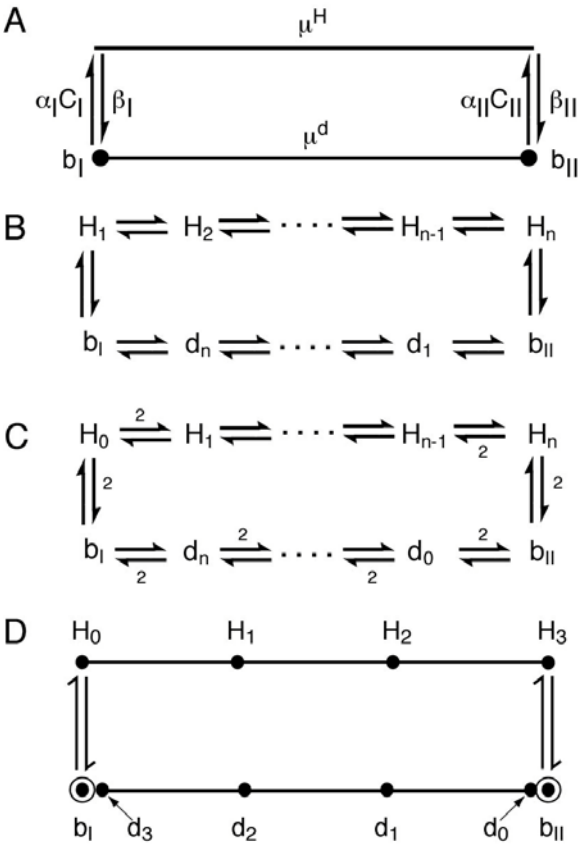

Figure 2. (A) State diagram for the lumped state approximation (LSA) of the single proton conduction mechanism. (B) State diagram of the n^{th} random walk leading to the LSA model. States H_i correspond to proton occupancy and d_i correspond to defect diffusion. States b_I and b_{II} model the boundary regions of Figure 1B. (C) State diagram for numerical computation of the LSA model. Escape rates from the endmost sites of the proton and defect diffusion intervals are multiplied by factors of 2 as indicated - the trapezoid rule. (D) Locations of the numerical random walk sites on the LSA state diagram for n=3. Boundary states are distinguished by surrounding circles.

Instead, the use of a single reaction coordinate assumes that the dynamics depends only on a single important degree of freedom. An analogy can be made with a ballet performance, where the positions and movements of the dancers at any moment are determined by the score. Of course, the atomic positions and orientations in a biomolecule would not progress steadily through a parameterized sequence of states, but the value of the parameter would change diffusively. Further, high frequency thermal motions with small amplitudes would be superimposed on the synchronized dynamics.

However, proton permeation through gramicidin may involve more than one significant degree of freedom. For example, even in the presence of an excess proton in the pore, the orientation of waters which are well separated from the center of excess charge is not rigidly constrained (7). The mechanism of proton escape may then be partially determined by the interaction between the center of excess charge and defects within the water chain. If the movements of the center of charge and of the defects are substantially independent, two or more degrees of freedom may be required to describe their interaction. A second example is provided by the RR dioxolane linked analogs of gramicidin (12-14). Molecular modeling suggests that the backbone carbonyls closest to the dimer interface can flip between orientations of almost equal energy, one projecting at an angle of 20-30° into the pore and the other projecting at an angle of 20-30° away from the pore (15). This conformational change alters the environment of cations in the pore and may need to be taken into account by a permeation model as a separate degree of freedom. This suggests that a satisfactory description of cation permeation through RR gramicidin may require a more complicated configuration space than a description of permeation through native gramicidin.

These considerations motivate the development of methods to construct and solve numerical framework models which can be more elaborate than the one dimensional models constructed so far (2,6,10,16). This article introduces a method which involves finding the steady states of a random walk constructed using a *trapezoid rule* closely related to the rule for numerical integration. It is first applied directly to the framework model described by ref. 2, where an analytical solution is available for comparison with our numerical result. This model simplifies the continuous families of transitions portrayed in Figure 1C using the lumped state approximation (6, 17). The numerical method is then used to construct a more elaborate model which directly incorporates the families of transitions; this is also compared with the analytical solutions based on the simplified diagram.

3. METHODS AND RESULTS

3.1. Lumped State Approximation Model

The state diagram of the lumped state approximation (LSA) of the single proton conduction mechanism is shown in Figure 2A, and is interpreted similarly as the simplified configuration space of Figure 1C. The top or proton segment parameterizes the diffusion of an excess proton through the pore and the bottom or defect segment parameterizes the diffusion of a defect mediating water reorientation. Mathematically, these are both described by Smoluchowski equations, which are diffusion equations that incorporate the systematic influence of the proton and water reorientation potentials of mean force. Their boundary conditions allow an excess proton to enter the pore with transition densities that are exponentially distributed in time when the channel is receptive. The exponential distribution also underlies rate theory models (for example, ref. 18) and is an appropriate approximation when the concentration of excess protons in the surrounding baths is not too large (16,19). The boundary regions of the defect segment are modeled as the

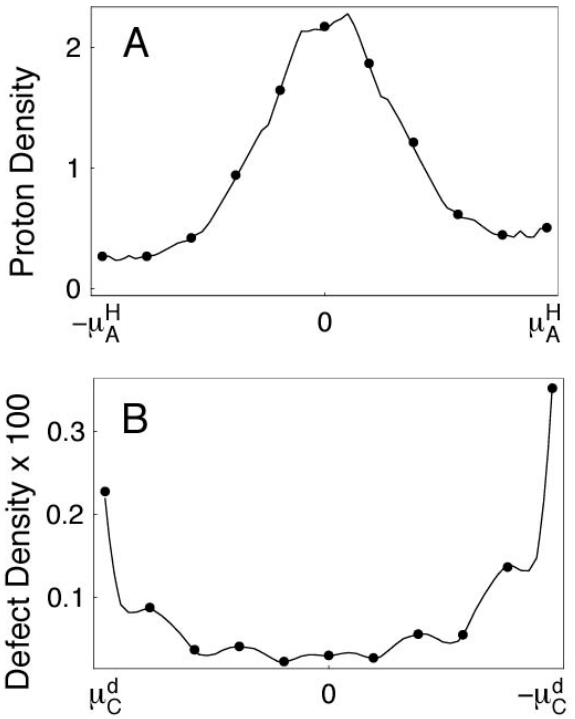

Figure 3. LSA proton and defect state probabilities for n=10. These were constructed for high symmetrical concentrations of proton in bulk, $C_I = C_{II} = 5M$, an applied transmembrane of $\Psi_I = 25.5$ mV (1 k_BT at 23°C) and the scaled PM6 potential given by the solid curve in Figure 1B (10). Dots are the numerical computation and the curve is the analytical LSA model. (A) Proton density. (B) Defect density.

lumped states b_I and b_{II}. The lumped state approximation neglects the time required for diffusion across the boundary regions, and is accurate as long as this is much shorter than the time required to diffuse over the central barrier on the defect segment (17). The approximation is used because it gives a model that can be solved analytically.

We constructed the LSA model as the limit of a sequence of random walks (10). The state diagram for the n^{th} random walk is shown in Figure 2B. The n random walk sites H_i, i=1…n, are the proton occupancy states and the n random walks sites d_i describe defect diffusion over the water reorientation barrier. The states b_I and b_{II} model the boundary regions. Transition probabilities between neighboring states are defined so that a coupled pair of Smoluchowski equations describing diffusion around the state diagram is obtained in the limit $n \to \infty$. This construction is required in order to obtain the boundary conditions described above. The coupled system of equations then describes either the diffusion of a single proton in the pore or water reorientation in an empty pore. The boundary conditions used by Goldman-Hodgkin-Katz theory (for example, ref. 18) or Poisson-Nernst-Planck theory (for example, ref. 20) lead to mathematical models which correspond to an infinite superposition of occupancy states (19). These *mean field* theories do not take into account correlations between ions and waters occupying the pore and are not appropriate for our purpose.

Below, we compare the analytical LSA results with numerical computation. Figure 2C shows the form of the numerical state diagrams. States H_0 and d_0 have been introduced, giving n+1 proton states and n+1 defect states. The transition probabilities depend on n in the same way as with the diagram shown in Figure 2B. However, the endmost sites, H_0, H_n, d_0 and d_n, have only half weight. The reason for this weighting is easy to understand. Consider the proton occupancy states. Each of the sites H_0, …, H_{n-1} may be viewed as corresponding to subintervals of the proton segment, in Figure 2A, centered at that site. The endmost random walk sites, H_0 and H_n, correspond to endmost subintervals of the proton segment that only have half the width of the others. Assigning these states half weight is analogous to the extended trapezoid rule used in numerical integration (for example, ref. 21). In the numerical model, the half weighting is achieved by multiplying the transition probabilities corresponding to escape from these states by a factor of two. These prefactors are indicated in Figure 2C. The location of the numerical random walk sites on the state diagram is indicated in Figure 2D for n = 3.

In the diffusion limit, $n \to \infty$, states $H_0,\ldots H_n$ converge to the proton segment on which a probability density is defined. States $d_0,\ldots d_n$ converge to the region of the defect segment between the boundary states on which a density is also defined. However, transitions between d_0 and the boundary state b_{II} and between d_n and the boundary state b_I scale with n differently than do transitions between states on the proton segment or the interior of the defect segment. In the diffusion limit, these boundary states become mathematical points associated with positive probability. They are distinguished by surrounding circles in Figure 2D.

The numerical solution of the LSA is achieved as the steady-state solution of the numerical random walk at a finite value of n. If we denote the probability of site i as Q_i and the transition probability from site i to neighboring site j as $k_{i,j}$, then the following equation is satisfied at steady state:

(1) $Q_{i-1}\, k_{i-1,i} + Q_{i+1}\, k_{i+1,i} = Q_i\, (k_{i,i-1} + k_{i,i+1})$.

There are 2 n + 4 such equations, one for each state in Figure 2C. One of these can be expressed as a linear combination of the others and is discarded. However, we must also include the normalization condition that the sum of all of the site probabilities Q_i is 1. This gives a linear system of 2 n + 4 algebraic equations which are solved simultaneously. For the examples below, this is achieved using the generic LinearSolve command in the software package Mathematica (version 4.1). The net current J clockwise around the state diagram can be calculated as

(2) $J = Q_i\, k_{i,i+1} - Q_{i+1}\, k_{i+1,i}$

for neighboring sites i and i+1.

Figure 3 compares the numerical and analytical state probability densities for protons in the occupied pore and defects mediating water reorientation in the empty pore. Gramicidin A parameter values are taken from optimal fits with the PM6 water reorientation barrier

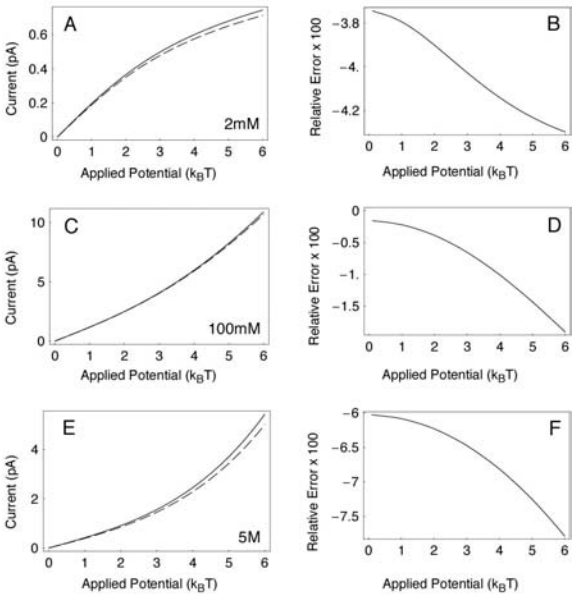

Figure 4. Comparison between analytical LSA currents and the n=10 numerical computation. Concentration in bulk are symmetrical and applied potentials are indicated on the abscissas. In the current panels on the left, the solid curves are the analytical results and the dashed curves are the numerical results. (A) Currents in picoAmps at 2mM. (B) Relative error at 2mM. (C) Currents at 100mM. (D) Relative error at 100mM. (E) Currents at 5M. (F) Relative error at 5M.

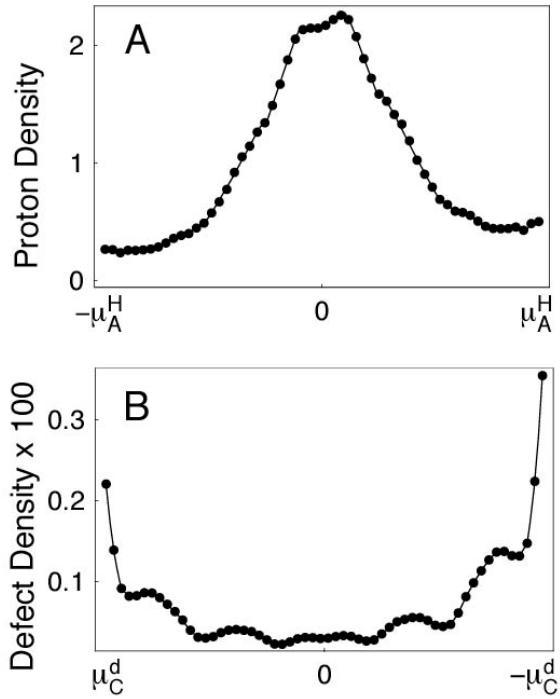

Figure 5. LSA proton and defect state probabilities for n=57 This figure was constructed under the same conditions as Figure 3. Dots are the numerical computation and the curve is the analytical LSA model. (A) Proton density. (B) Defect Density.

reduced in amplitude by 2 kcal/mol (2), shown as the solid curve in Figure 1B. In Figure 3, the analytical results are given by the solid curve and the numerical results by filled circles. This figure was constructed assuming very high symmetrical concentrations of excess protons in the bulk: $C_I = C_{II} = 5M$ and a transmembrane potential of $\Psi_I = 25.5mV$ (1 k_BT at 23° C). Under these conditions, the probability that a proton occupies the pore is nearly one. The numerical results of the endmost sites are multiplied by a factor of two for display in the figure, since their weights are reduced by this factor according to the trapezoid rule. The relative errors quoted below are given by

(3) relative error = (numerical result – analytical result) / analytical result .

The results shown in Figure 3 correspond to the numerical calculation with n = 10 in the state diagram of Figure 2C. The relative error in the integrated proton density is $-1.3\ 10^{-4}$, but there is a much bigger relative error in the integrated defect density, 0.18. The integrated defect density is very small, and corresponds to the probability that, at a given time, the channel will be found with an empty pore and a water reorientation defect diffusing between the boundary regions of Figure 1B (solid curve). Its large relative error can be understood from Figure 3B. The density increases rapidly toward the endpoints, which are sites of the numerical calculation. The density at these endpoints is much greater than the average value in an appropriate neighborhood interior to these points. In contrast, the relative errors for the probabilities of the boundary states are much smaller, that for b_I is -0.0045 and that of b_{II} is 0.017.

We are ultimately interested in model currents, since these numbers would be compared with experiments. Figure 4 compares the analytic LSA currents with numerical values for n = 10. Currents are given in the left hand panels and their relative errors in the right hand panels. For each current panel, the voltage is given on the abscissa, in units of $k_BT = 25.5mV$, and current is given on the ordinate, in picoAmps (pA). The solid curve shows the results of the analytical LSA model and the dashed curve the results of the numerical model. The top row corresponds to symmetrical concentrations of 2mM excess protons in the bulk, the middle row to concentrations of 100mM, and the bottom row to concentrations of 5M. The largest relative errors are encountered for the high concentration case. Their density profiles at $\Psi_I = 25.5mV$ were given in Figure 3.

Figure 5 shows results of the numerical LSA model with n = 57, a value that corresponds to one random walk site at each reaction coordinate value between the boundary regions where the molecular dynamics simulations evaluated the water reorientation potential of mean force. The relative error of the integrated proton density is $-3.2\ 10^{-6}$ and that of the integrated defect density is 0.0042. These errors are smaller by a factor of about 40 compared with those obtained for n=10. The relative error for b_I is –0.0021 and that of b_{II} is 0.0017.

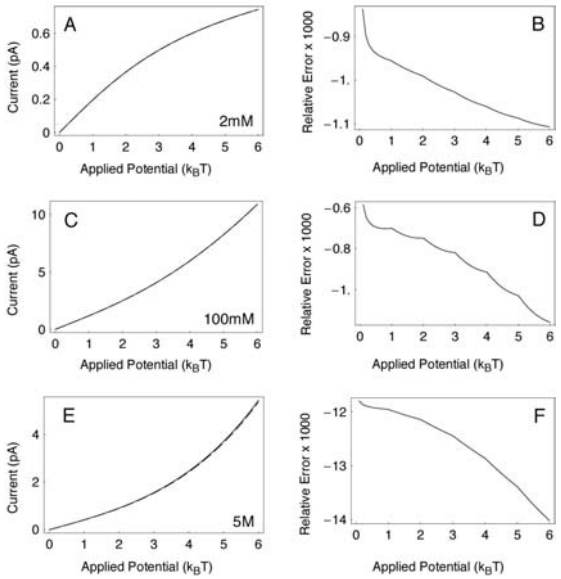

Figure 6. Comparison between analytical LSA currents and the n=57 numerical computation. Panels are interpreted in the same way as for Figure 4. (A) Currents at 2mM. (B) Relative error at 2mM. (C) Currents at 100mM. (D) Relative error at 100mM. (E) Currents at 5M. (F) Relative error at 5M.

Figure 6 shows the corresponding currents for n=57. At symmetrical concentrations of 2mM, the relative error has decreased by a factor of 40 compared with the currents for n = 10. Relative errors at 100mM are comparable to those at 2mM. However, the errors are an order of a magnitude greater at 5M, and have decreased only by about a factor of 5 compared with those at n=10.

The time required for a current evaluation may potentially limit the analyses that can be performed to compare models with experiment. The sensitivity analysis presented by (2) required over 10^6 current evaluations. Evaluation of the analytical formula for the LSA current is very fast. Tables are pre-computed to allow rapid evaluation of integrals. On a 1 GHz Pentium III machine running the Mathematica software package, a current evaluation requires only $5\ 10^{-4}$ seconds. To solve the LSA model numerically for n = 57 requires the solution of a linear system of 2n+4=118 equations. Using the LinearSolve command, this takes 0.017 second, about 35 times longer than the analytical solution.

3.2. Constant entrance probability model

The model of proton conduction suggested by Figure 1C includes families of transitions from the proton-occupied pore to the empty (occupied only by waters) pore. This is because the dipole moment of the empty pore will not be uniquely determined after a proton leaves through a channel entrance. Especially near the opposite end of the channel, the pore waters will be left in a distribution of states. This distribution could be estimated by molecular dynamics. An excess proton at a channel entrance might be removed in repeated simulations, sampling the distribution of remaining pore water dipole moments. The intervals of remaining pore water states in the empty pore are the boundary regions. The LSA simplifies these dynamics, which cannot be parameterized by a single reaction coordinate, by lumping the boundary regions into single points b_I and b_{II} on the state diagram of Figure 2A.

This section introduces a the Constant Entrance Probability (CEP) model of proton conduction which instead explicitly incorporates the boundary regions. Like the LSA model, it is obtained as the limit of a sequence of random walks. The n^{th} member of this sequence is shown in Figure 7. The states denoted H_i model proton diffusion through the pore and the states denoted d_i model water reorientation. H_0 models an excess proton at the channel entrance on side I and is coupled to m+1 water reorientation states which model the boundary region on side I. Similarly, H_n is coupled to m+1 states which model the boundary region on side II. The ratios of the entrance to exit rates are determined, through the thermodynamic principle of detailed balance, by the energy differences between states in the boundary regions and states H_0 and H_n. These ratios vary throughout the boundary regions as the energy differences themselves vary; see Figure 1B. In the CEP model, the rate of proton entrance is assumed to be constant within the boundary regions and the rate of proton exit varies.

When the limit $n \rightarrow \infty$ is taken, we obtain the system of differential equations and boundary conditions for the CEP model, whose state diagram is effectively Figure 1C. The top segment parameterizes the diffusion of a proton through the pore, described by a Smoluchowski equation as with the LSA model. Proton entrance and exit are described only through the endpoints of the top segment, again similar to the LSA model. Diffusion of the water reorientation reaction coordinate across the central barrier, between the boundary regions of the bottom segment, is also described by a Smoluchowski equation. However, two additional terms appear in the diffusion equations modeling transport in the boundary regions. These describe densities of transitions to and from the boundary regions and the endpoints of the proton segment. Corresponding to these two densities, two integrals over the boundary regions appear in the boundary conditions for the Smoluchowski equation on the proton segment.

The CEP model is approximated numerically by computing the steady state properties of the random walk shown in Figure 7. With the transition probability prefactors shown, and further described by the figure legend, the integrals that appear in the proton segment boundary conditions are approximated as Riemann sums by the trapezoid rule for numerical integration (21). Steady states are computed as the solution of a linear system of 2n+2 equations, one for each of the states, H_i and d_i, shown in Figure 7. There is an analytical relationship between the CEP and LSA models, and CEP parameters values were chosen to correspond to the LSA computations shown previously.

Figure 8 compares the CEP and analytical LSA probability densities for protons in the occupied pore and

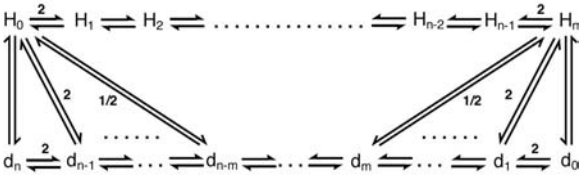

Figure 7. State diagram for numerical computation of the CEP model. States H_i correspond to proton occupancy and d_i correspond to defect diffusion. The m+1 transitions between the state H_0 and the defect segment model the family of transitions on side I of the channel in Figure 1C. The m+1 transitions between state H_n and the defect segment model the family of transitions on side II. Escape rates from the endmost sites of the proton and defect segments are multiplied by factors of 2, with the following exceptions. Rates directly between the endmost sites are not multiplied by prefactors and rates between H_n and d_m and between H_0 and d_{n-m} are multiplied by the prefactors indicated (when no prefactor is shown, its value is 1). In the limit $n \rightarrow \infty$, an analytical model is obtained whose state diagram is Figure 1C.

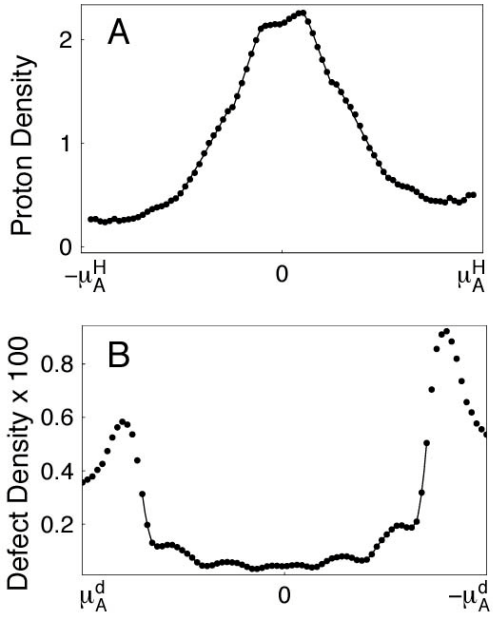

Figure 8. CEP proton and defect state probabilities for n=81 and m=12. As in Figure 3 and 5, these were constructed for $C_I = C_{II} = 5M$, and $\Psi_I = 25.5$ mV and using the scaled PM6 potentials. Dots are the numerical computation and the curve is the analytical LSA model. A. Proton density. B. Defect density. Compared to Figure 3 and 5, the defect diffusion interval has been extended to include the boundary regions. The LSA solution is defined over$[-\mu_C^d, \mu_C^d]$.

defects mediating water reorientation. The numerical results are computed for n = 81 and m=12, corresponding to one random walk site at each reaction coordinate value of the defect segment, including the boundary regions. The LSA results are given by the solid curve and the CEP results by filled circles. Increasing values of the reaction coordinates μ^H and μ^d correspond to progress clockwise around the diagram of Figure 1C. Conditions again correspond to high symmetrical concentrations of excess protons in the bulk: $C_I = C_{II} = 5M$ and $\Psi_I = 25.5$mV. CEP results for the endmost sites are multiplied by two, since their weights are reduced by this factor in the trapezoid rule. The relative error is defined by Eq. (3). That of the integrated proton probability density is $-5\ 10^{-6}$ and that of the integrated defect density between the boundary regions is 0.0040. The relative error between the integrated CEP boundary region I density and the weight of LSA boundary state b_I is $-7\ 10^{-4}$, and the corresponding error on side II is 0.0024. These last two comparisons suggest that the lumped state approximation works very well under the conditions of these computations.

Figure 9 compares the numerical CEP currents for n=81 with those computed using the analytical LSA model. Panels are arranged as in Figure 4 and 6. Relative errors are comparable to those obtained from the numerical LSA model with n=57; compare with Figure 6. As with the LSA computations, the relative errors are largest at high proton concentrations. Each CEP current evaluation requires the solution of a linear system of 2n+2 = 164 equations. Using Mathematica on the 1 GHz Pentium III machine, an evaluation requires 0.032 seconds, a factor of 64 greater than required by the analytical LSA model.

4. SUMMARY AND DISCUSSION

This article has described numerical methods for constructing framework models of single proton permeation through gramicidin. Numerical LSA models are first constructed, based on the trapezoid rule which is described in the text in section 3.1 that discusses Figure 2C and 2D. These numerical models are compared with the analytical model (2) using the relative error defined by Eq. 3. For n = 10, the relative errors of the numerical currents are under 5% for symmetrical $[H^+]$ of 100mM or less and transmembrane potentials of 150mV or less. This includes the range of apparent single proton conduction in gramicidin A. The 5% relative error in the current value is much less than that expected from molecular dynamics due to uncertainty in PMFs and diffusion coefficients. For n = 57 the relative error of the numerical LSA model decreases by a factor of about 5 at symmetrical $[H^+]$=5M and by a factor of about 40 for $[H^+]$ = 100mM or less.

The numerical methods also allow construction of the CEP model, which explicitly models the continuous families of transitions between the proton occupied pore and the empty pore indicated in Figure 1C. The CEP model has an analytical relationship with the LSA model which allows the identification of corresponding parameter values. Using these, the comparison between CEP and the analytical LSA currents is as close as between the n = 57 LSA and analytical models. This result reinforces the conclusions of a previous study (17), which showed the mean first passage times for diffusion across a potential barrier using the lumped state approximation closely matched those in the absence of the approximation, so long as the potential barrier had an amplitude greater than 2 k_BT

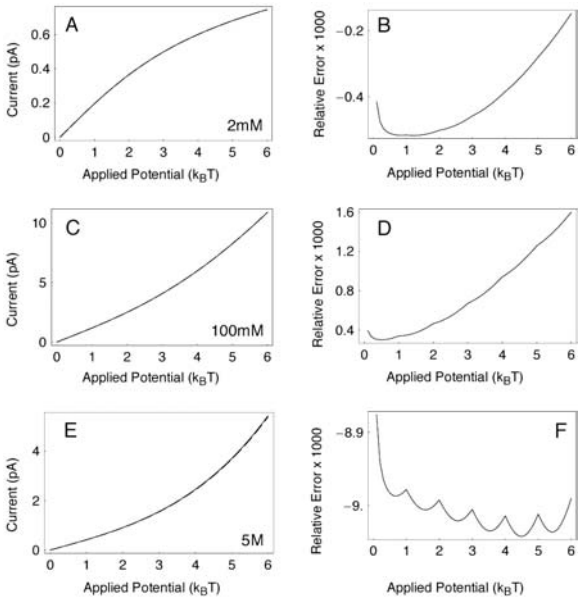

Figure 9. Comparison between analytical LSA currents and the numerical CEP computation. Panels are interpreted as in Figure 4 and 6. (A) Currents at 2mM. (B) Relative error at 2mM. (C) Currents at 100mM. (D) Relative error at 100mM. (E) Currents at 5M. (F) Relative error at 5M.

and the boundary regions were not too wide. The construction of the CEP model also demonstrates that the numerical methods can construct framework models that would be difficult or impossible to solve analytically.

Framework models have been constructed to describe the permeation of single Na^+ ions (16) and single protons (2) through gramicidin. These models describe the dynamics of permeation in simplified configuration spaces that are designed to incorporate potentials of mean force and diffusion coefficients calculated by the molecular dynamics simulations. The accuracy of the energies obtained by MD is controversial (22). However, the close comparison between the water reorientation potential whose amplitude was reduced to allow a detailed fit to conductance data (2) and the potential of mean force calculated using TIP3P waters (1) in Figure 1B (dashed curve) is very attractive. The difference between the original MD results for PM6 and TIP3P waters may suggest the uncertainty that remains. The use of PMFs and diffusion coefficients calculated from MD means that the framework models implicitly take into account the detailed interactions between a permeating ion, the channel and pore waters. The comparison with experimental conductances provides both insight into permeation mechanisms and feedback that can be used to refine the MD. However, the framework models of Na^+ and H^+ permeation through gramicidin depend on the assumption that the dynamics of permeation are so constrained that they can be reasonably projected onto a single reaction coordinate.

Brownian dynamics simulations have also been used to fit potential profiles and diffusion coefficients to gramicidin conductance data (23). This method does not assume that the dynamics of permeation are highly constrained. Moreover, it does take into account correlations between ions, which mean field theories of ion permeation do not (19,24-25). However, Brownian dynamics does not incorporate the detailed description of the ions and the channel found in molecular dynamics, and water molecules are not modeled individually at all. These details may be very important for understanding permeation through narrow ion channels in which ions and waters must be ordered in single file. For example, a cation in the channel reorients neighboring water molecules so that, on average, partial negative charges are directed towards the cation (7). This may well influence the energetics of a second ion trying to enter the pore. In addition, the energetics of the doubly occupied state depend on how water molecules pack between the ions at their binding sites (26).

An attempt to model these interactions by Brownian dynamics simulations would involve the introduction of additional empirical forces acting on the ions, including free parameters. Optimizing the values of those parameters would require comparing model currents with experimental data. In the Brownian dynamics simulations (23), the computations to complete a simulation period of 1 μsec required 30 hours CPU on a supercomputer. In 1 μs, only a net 6 elementary charges pass through the channel at a current of 1 pA. In contrast, an evaluation of the analytical LSA currents takes 5 10^{-4} seconds on a 1 GHz desktop PC, allowing an extensive comparison between model currents and conductance data in the free parameter space that required more than 10^6 current evaluations (2). The time required for the evaluation of numerical framework model currents is longer, but remains short enough to allow an extensive comparison between model and experiment.

Framework models make the assumption that the dynamics of ion permeation, which involve thousands of degrees of freedom in molecular dynamics simulations, can be reasonably projected onto simplified configuration spaces with a small number of degrees of freedom. This assumption was motivated, in part, by the empirical success of rate theory (for example, ref. 18), which framework models generalize. The framework approach has provided a simple explanation for a large set of proton conductance data from gramicidin A and two analogs, which is consistent with independent calculations (2). However, there may also be a theoretical justification for projection onto a simplified configuration space.

Dynamics described by complicated systems of ordinary differential equations or by partial differential equations can sometimes be shown to be controlled, in a clear mathematical sense, by much simpler equations. The number of essential degrees of freedom in these simpler equations is related to the concept of dimension in nonlinear dynamics. Strogatz (27) gives a wonderful introduction to the point of view of nonlinear dynamics and the concept of dimension. Schreiber (28) reviews methods developed to estimate dimension from experimental data. However, these depend heavily on the use of time delayed

coordinates, which do not handle the thermal noise which dominates the dynamics of molecular systems well.

Fortunately, a related sense of dimension seems to emerge from principal coordinate analysis, which has already been introduced to the study of molecular dynamics simulations of protein folding (29,30). Snapshots of a simulation correspond to a set of points in the high-dimensional configuration space of a selected group of atoms within the simulation. Projections of these points to lines through the centroid of the set are considered. That which gives the greatest variance is the first principal coordinate. It corresponds to the degree of freedom (a synchronized trajectory which may involve all of the atoms in the system) which moves the most in the simulation. The process is repeated to obtain the line orthogonal to the first coordinate with the greatest variance, and so forth.

Principal coordinate analysis has already been applied to the analysis of the fluctuations of water filled gramicidin (31). It was found that 70-80% of the fluctuations in the pore direction were due to the correlated movement of the whole water column. This result suggests that an analysis of water permeation through gramicidin which refers only to this one degree of freedom would be appropriate. However, the number of essential coordinates required to describe the permeation process is likely to increase as the channel environment is made more complex (13, 15) or as the pore radius increases (32). The development of numerical methods for constructing framework models would then be required to apply this approach to the description of these more complex molecular motions.

5. ACKNOWLEDGMENT

The author thanks David Busath and Regis Pomès for many discussions concerning the structure and dynamics of gramicidin A and its analogs. He also thanks Regis Pomès for sharing the TIP3P profile which is the dashed curve in Figure 1B. Conversations with Benoit Roux motivated construction of the CEP model.

6. REFERENCES

1. Pomès R, Roux B: Molecular mechanism of H^+ conduction in the single-file water chain of the gramicidin channel., *Biophys J,* 82, 2304-2316 (2002)

2. Gowen JA, Markham JC, Morrison SE, Cross TA, Busath DD, Mapes EJ, Schumaker MF: The role of Trp side chains in tuning single proton conduction through gramicidin channels, *Biophys J,* 83, 880-98. (2002)

3. Arseniev AS, Barsukov IL, Bystrov VF, Lomize AL, Ovchinnikov Yu A: 1H-NMR study of gramicidin A transmembrane ion channel. Head-to-head right-handed, single-stranded helices, *FEBS Lett,* 186, 168-74 (1985)

4. Ketchem RR, Roux B, Cross TA: High-resolution polypeptide structure in a lamellar phase lipid environment from solid state NMR derived orientational constraints, *Structure,* 5, 1655-1669 (1997)

5. DeCoursey T: Voltage-gated proton channels and other proton transfer pathways, *Physiol Rev*, 83, 475-579 (2003)

6. Schumaker MF, Pomes R, Roux B: A combined molecular dynamics and diffusion model of single proton conduction through gramicidin, *Biophys J,* 79, 2840-2857 (2000)

7. Pomès R, Roux B: Structure and dynamics of a proton wire: a theoretical study of H^+ translocation along the single-file water chain in the gramicidin A channel, *Biophys J,* 71, 19-39 (1996)

8. Pomes R: Theoretical studies of the Grotthuss mechanism in biological proton wires, *Israel J Chem,* 39, 387-395 (1999)

9. Phillips LR, Cole CD, Hendershot RJ, Cotten M, Cross TA, Busath DD: Noncontact dipole effects on channel permeation. III. Anomalous proton conductance effects in gramicidin, *Biophys J,* 77, 2492-501 (1999)

10. Schumaker MF, Pomès R, Roux B: A framework model for single proton conduction through gramicidin, *Biophys. J.,* 80, 12-30 (2001)

11. Anderson D, Shirts RB, Cross TA, Busath DD: Non-contact dipole effects on channel permeation V. Computed potentials for fluorinated gramicidin., *Biophys J,* 81, 1255-1264 (2001)

12. Stankovic CJ, Heinemann SH, Delfino JM, Sigworth FJ, Schreiber SL: Transmembrane channels based on tartaric acid-gramicidin A hybrids, *Science,* 244, 813-817 (1989)

13. Quigley EP, Quigley P, Crumrine DS, Cukierman S: The conduction of protons in different stereoisomers of dioxolane- linked gramicidin A channels, *Biophys J,* 77, 2479-91 (1999)

14. Cukierman S: Proton mobilities in water and in different stereoisomers of covalently linked gramicidin A channels, *Biophys J,* 78, 1825-34 (2000)

15. Yu C-H, Cukierman C, Pomès, R: Theoretical study and the structure and dynamic fluctuations of dioxolane-linked gramicidin channels, *Biophys J*, 84, 816-831 (2003)

16. McGill P, Schumaker MF: Boundary conditions for single-ion diffusion, *Biophys J,* 71, 1723-42 (1996)

17. Mapes E, Schumaker MF: Mean first passage times across a potential barrier in the lumped state approximation, *J Chem Phys,* 114, 76-83 (2001)

18. Hille B, Ionic Channels of Excitable Membranes, 2nd ed., Vol. , Sinauer Associates, Inc., Sunderland, Massachusetts (1992)

19. Schumaker MF: Boundary conditions and trajectories of diffusion processes, *J Chem Phys,* 117, 2469-2473 (2002)

20. Chen D, Lear J, Eisenberg B: Permeation through an open channel: Poisson-Nernst-Planck theory of a synthetic ionic channel, *Biophys J,* 72, 97-116 (1997)

21. Press WH, Teukolsky SA, Vetterling WT, Flannery BP: Numerical Recipes in Fortran, 2nd ed., Cambridge University Press, New York (1992)

22. Allen TW, Bastug T, Kuyucak S, Chung S-H: Gramicidin A as a test ground for molecular dynamics force fields, *Biophys J*, 84, 2159-2168 (2003)

23. Edwards S, Corry B, Kuyucak S, Chung S-H: Continuum electrostatics fails to describe ion permeation in the gramicidin channel, *Biophys J,* 83, 1348-1360 (2002)

24. Moy G, Corry B, Kuyucak S, Chung S-H: Tests of continuum theories as models of ion channels. I. Poisson-Boltzmann theory versus Brownian dynamics, *Biophys J,* 78, 2349-63 (2000)

25. Corry B, Kuyucak S, Chung S-H: Tests of continuum theories as models of ion channels. II. Poisson-Nernst-Planck theory versus Brownian dynamics, *Biophys J,* 78, 2364-81 (2000)

26. Roux B, Prod'hom B, Karplus M: Ion transport in the gramicidin channel: molecular dynamics study of single and double occupancy, *Biophys J,* 68, 876-92 (1995)

27. Strogatz S: Nonlinear Dynamics and Chaos, Perseus Books, Cambridge, MA (1994)

28. Schreiber T: Interdisciplinary application of nonlinear time series methods, *Phys Reports,* 308, 1-64 (1999)

29. Garcia A: Large-amplitude nonlinear motions in proteins, *Phys Rev Lett,* 68, 2696-2699 (1992)

30. Amadei A, Linssen ABM, Berendsen HJC: Essential dynamics of proteins, *Proteins,* 17, 412-425 (1993)

31. de Groot BL, Tieleman DP, Pohl P, Grubmüller H: Water permeation through gramicidin A: desformylation and the double helix: a molecular dynamics study, *Biophys J,* 82, 2934-2942 (2002)

32. Brewer ML, Schmitt UW, Voth GA: The formation and dynamics of proton wires in channel environments, *Biophys J,* 80, 1691-702. (2001)

Key Words: Framework Model, Gramicidin, Lumped State, Molecular Dynamics, Proton Conduction

Send correspondence to: Dr Mark F. Schumaker, Department of Mathematics and Center for Integrated Biotechnology, Washington State University, Pullman WA 99164-3113, Tel: 509-335-7273, Fax: 509-335-1188, E-mail: schumaker@wsu.edu